IOSR Journal of Mechanical and Civil Engineering (IOSR-JMCE)
e-ISSN: 2278-1684,p-ISSN: 2320-334X, Volume 14, Issue 6 Ver. I (Nov. - Dec. 2017), PP 85-91
www.iosrjournals.org

Welding Deformation of a Rectangular Box during Gas Metal Arc Welding

Pham Son Minh [1], Tran Thanh Phong [1]
[1]*University of Technology and Education Ho Chi Minh City, HCM City, Vietnam*

Abstract: *This paper studies the welding deformation of a rectangular box in simulation and experiments. The box structure was modeled and simulated in ANSYS software using the thermoelastic-plastic approach. The box was constructed from four plates using four welders. The simulation results were verified in a series of experiments with four welding processes (two processes with single welders and two with double welders). The parent metal was low-carbon steel AISI 1005, and power was sourced from digital gas metal arc welding (GMAW) with a premixed shielding gas. The GMAW was affixed by the one-sided clamping technique. The thermoelastic-plastic 3D finite-element method analysis qualitatively agreed with the experimental results. Because it applied a symmetric stress, the double welder introduced less distortion than the single welder. In all processes, the deformation was severest at the plate corners and minimized at the center.*

Keywords: *Welding simulation, structure deformation, heat transfer, plate connection, plate distortion*

Date of Submission: 15 -11-2017 Date of acceptance: 30-11-2017

I. Introduction

The popularity of virtual manufacturing has increased in recent years, especially in important technical disciplines such as welding. The welding process connects metal parts to create a product. When joining welding structures in industry, a filler material is usually added to the metal plate as new weld passes. Thin metal-plate connections are often formed by the single-pass welding process. Predicting structure deformation is one of the most important issues in the welding industry and is often solved experimentally by the weld designer.

Structural deformation can also be predicted by numerical methods, but the welding structure is not easily modeled by the finite-element method (FEM). Because the heat is intensely concentrated in the heat source of welding, the clamping force, heat transfer, heating source, and other factors are subjected to many boundary conditions in regions near the weld line. Therefore, predicting three-dimensional weld deformations is of major interest in welding various engineering alloys.

Owing to recent developments in computing capabilities, the residual stresses in welded metals can now be predicted in three-dimensional simulations of the arc welding process. Many researchers have studied the thermal distributions and residual stresses in welded materials. For instance, Teng et al. [1] studied the residual stresses in multi-pass arc welding of steel pipes using finite-element (FE) techniques. They also discussed the effects of pipe diameter and wall thickness on these stresses. The authors of [2] improved the prediction accuracy of the thermos-mechanical model by adaptive mesh refinements that transported the results between different meshes. They compared their computed distortions and residual stresses with experimental measurements. Buttwelding of stainless steel pipes has been simulated in a nonlinear thermo-mechanical FE analysis [3]. This study revealed the axial and hoop stresses and their sensitivity to variations in the weld parameters. Many researchers have combined analytical and experimental methods to analyze the residual stresses in pipes joined by a girth-butt weld [4–7].

To model the metal filler for the welder [8–9], the present authors adopt the element "birth" and "death" FE technique, which controls the process step by step. The present study aims to develop an efficient method that reduces the design time and improves the accuracy of welding structure manufacturing. The product is modeled as a rectangular box. The model analyzes both the material properties and the welding zone situation. The local inherent stress of the welding bead is represented by an equivalent moment and other parameters, and the welding deformation is predicted by a newly proposed welding simulation implemented in ANSYS software.

II. Simulation and Experiment

Figure 1 overviews the simulation components of gas metal arc welding (GMAW). First, the welding process is designed following the American Welding Society standards. The welding geometry is then created in the research model. The welding models are meshed, and the boundary conditions are set up. All these data are

used in the simulations. The software outputs the temperature distribution, deformation, and residual stress of all welding structures.

Thermal evolution is a complex process associated with GMAW. The shape of the weld pool can be largely influenced by the weld-metal transfer mode and corresponding fluid flow dynamics [9]. In FE studies, GMAW is most commonly represented by the double-heat-source model presented by Goldak et al. [10] (see Figure 2). Table 1 lists the parameters of Goldak's model used in the present study. The chemical components and room-temperature mechanical properties of low-carbon steel are shown in Tables 2 and 3, respectively.

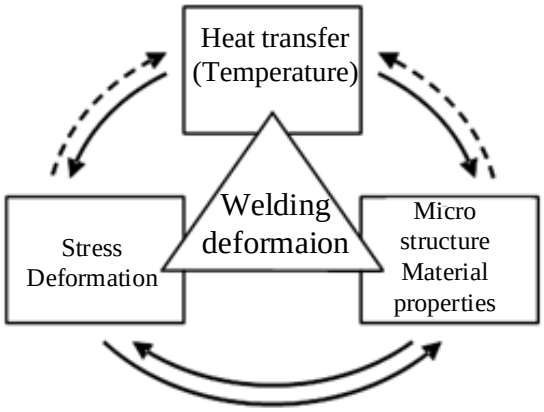

Figure 1. Components and their interconnections in the welding deformation simulation.

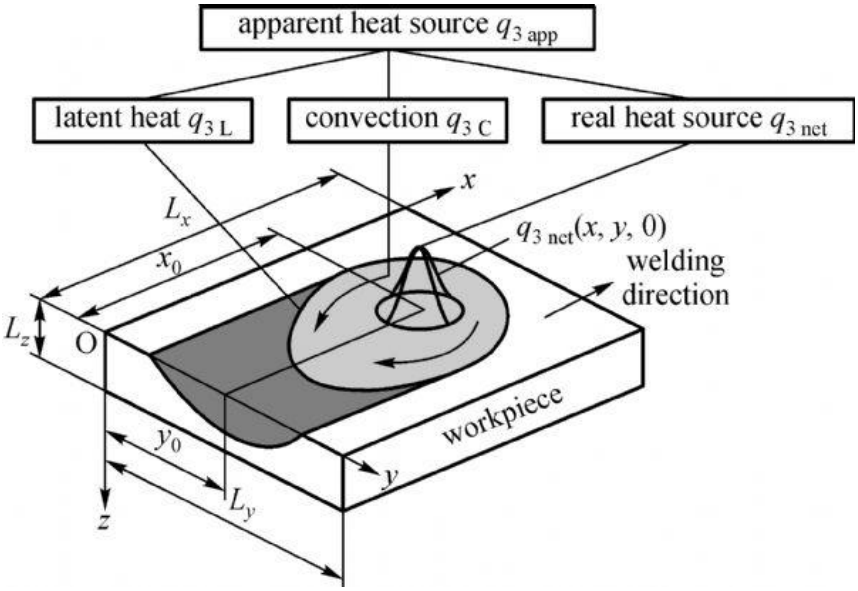

Figure 2. Overview of Goldak's double-heat-source model [10].

Table 1. Parameters of Goldak's double-heat-source model used in the present study.

Parameters of Goldak's double ellipsoid	
a_f	4.0 mm
a_r	7.0 mm
b	3.5 mm
d	3.0 mm

Table 2. Constituents of the low-carbon steel used in this study [11].

Standard	AISI 1005
% C	0.14–0.22
% Si	0.12–0.30
% Mn	0.40–0.65

Table 3. Material properties of the welding plates used in this study [11].

Material properties	
Young's Modulus at 20 °C	210 GPa
Minimum yield strength	355 MPa
Poisson's ratio	0.33
Solidus temperature	1404 °C
Liquidus temperature	1505 °C

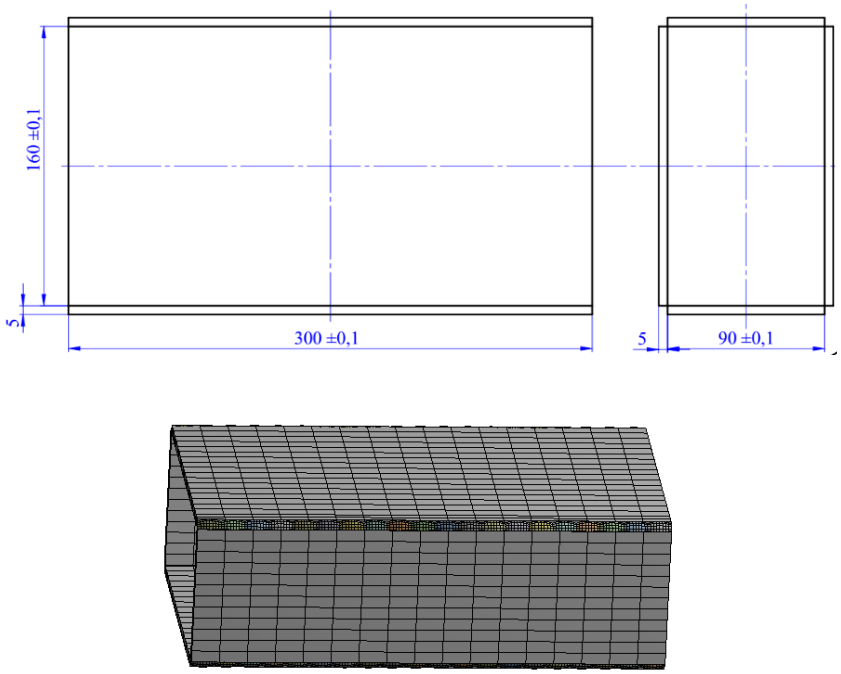

Figure 3. Dimensions and mesh model assumed in the simulations.

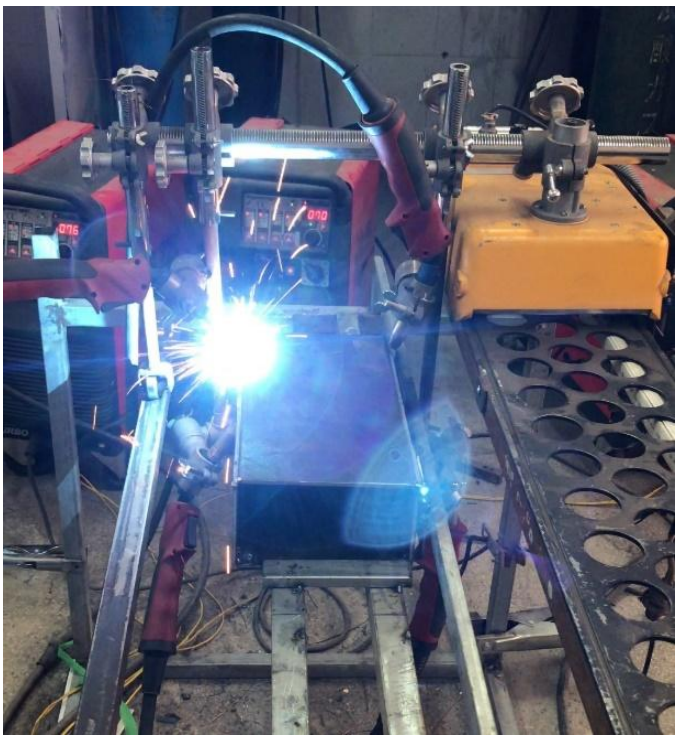

Figure 4. Experimental equipment.

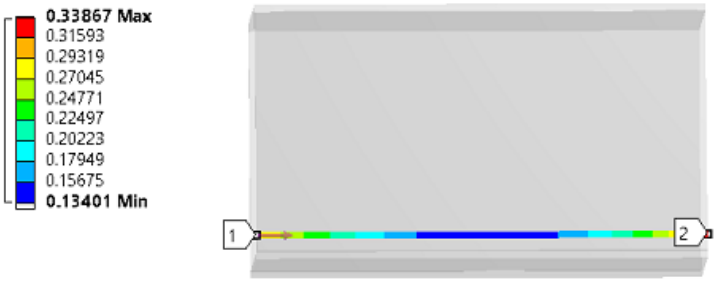

Figure 5. Cross-sectional observation of the welding deformation.

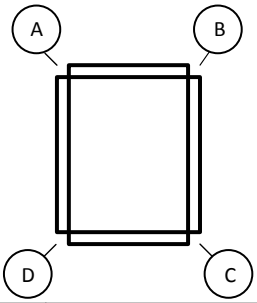

Process	Welding direction
1A Single Welder	A → B → C → D
1B Single Welder	A → C → B → D
2A Double Welders	A D → B C
2B Double Wleder	A B → C D

Figure 6. Welding processes.

Figure 3 shows the mesh model of the box in the established 3D solid model. The mesh is refined around the weld path and coarser at locations far from the weld. The initial condition is the preheating temperature, and all nodes of based plate are loaded, except for fillers. The accuracy of the simulation result was verified in a welding experiment (Figure 4). Because the experimental equipment could simultaneously operate at four welding locations, the influence of the welding step was well clarified. To estimate the quality of the welding process, the deformation was measured along the box face as shown in Figure 5. Moreover, the structural deformation was experimentally and numerically evaluated in four welding processes (described in Figure 6), revealing the effect of the welding process on deformation.

The welding process was simulated by the linear elastic shrinkage method, implemented in a relatively new FEM module from ANSYS. The welding distortion was predicted in a 5-mm thick corner joint. The

verification experiments were conducted on a fully automated welding system with a GMAW power source. The shielding gas for the welding process was carbon dioxide (CO_2). The initial and final dimensions of the specimen were measured by a coordinate measuring machine. The experimental welding parameters are given in Table 4. The single-welder processes (processes 1A and 1B in Figure 6) differed only in their welding order. The double-welder processes (processes 2A and 2B in Figure 6) differed only in the direction of welding.

Table 4. Welding parameters used in the simulation and experiments.

Welding parameter	Value
Current	90 A
Voltage	21.6 V
Welding speed	5.7 mm/s

III. Results and Discussion

Panels (a) and (b) of Figure 7 show the simulated deformations of the box at the end of each welding cycle outlined in Figure 6. The deformation was almost independent of the welding process. The deformation was lowest at the center of each plate and highest at the plate corner. This result is attributable to the heat concentration at the corner and the termination of the welding step at the corner. The temperature distribution also largely changes across the plate, being highest at the position of the final welding step. This result explains the residual stress differences among the processes. In processes 1A and 1B, the highest stress is located at site D, which is last visited by the welder. In processes 2A and 2B, the stress is concentrated along CD and BC, respectively, again reflecting the last processes of the welders.

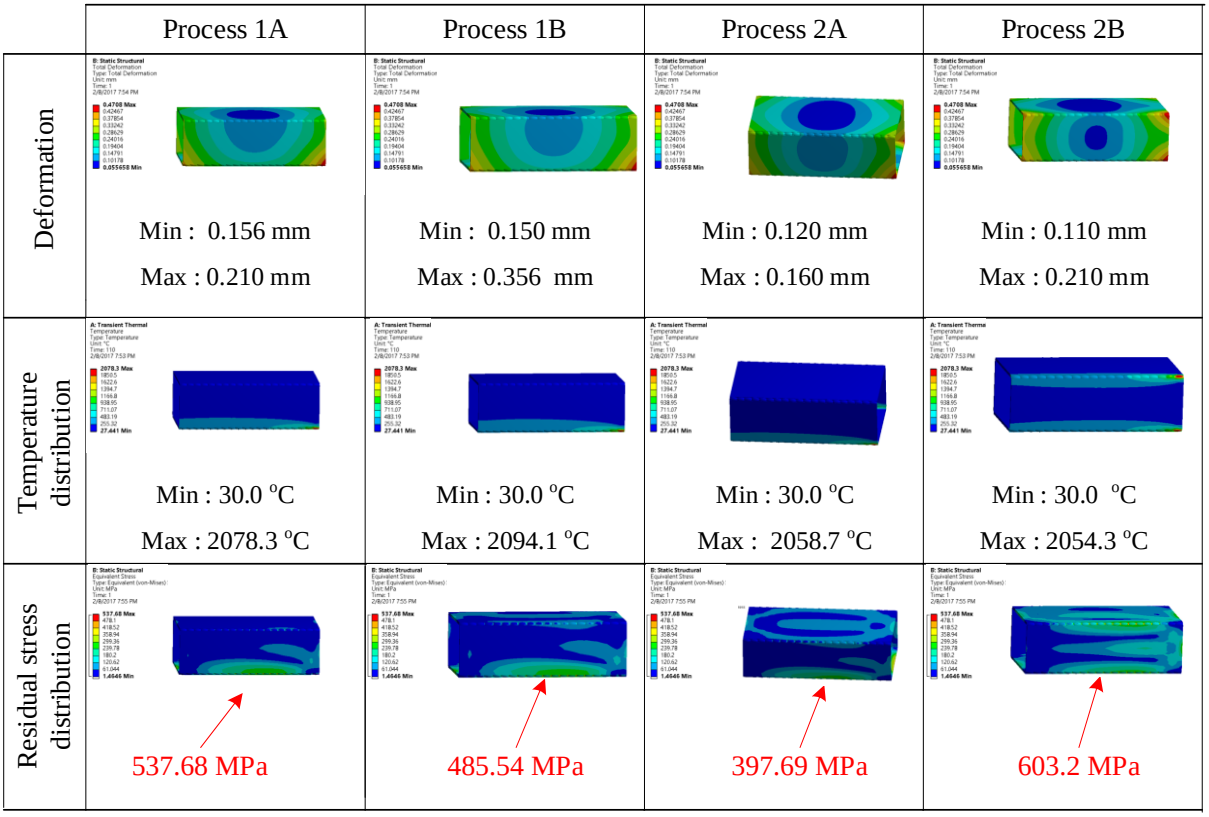

Figure 7. Simulation results at the end of the welding cycle.

The deformations varied among the four processes. More specifically, the deformation ranges in processes 1A, 1B, 2A, and 2B were 0.156–0.210, 0.150–0.356, 0.120–0.160, and 0.110–0.210 mm, respectively. Accordingly, the double welder causes less deformation than the single welder, possibly because the stress was applied symmetrically and simultaneously. Such symmetric stresses will probably reduce each other, lowering the overall stress and the structural deformation (Figure 7). The smallest deformation was observed in case 2A, which doubly welds AD and BC.

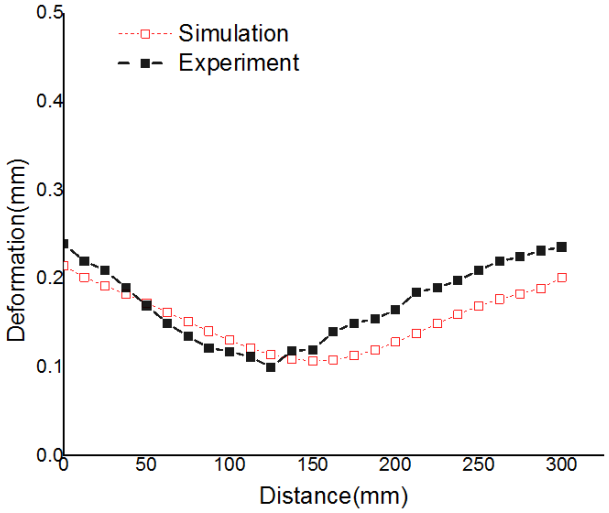

Figure 8. Simulated plate deformation in process 1A.

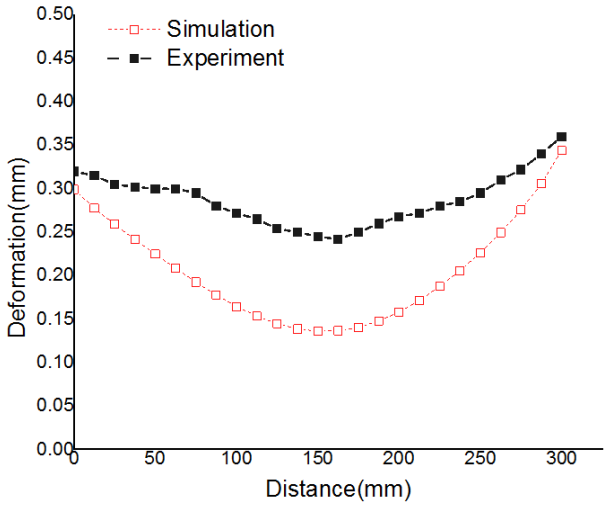

Figure 9. Simulated plate deformation in process 1B.

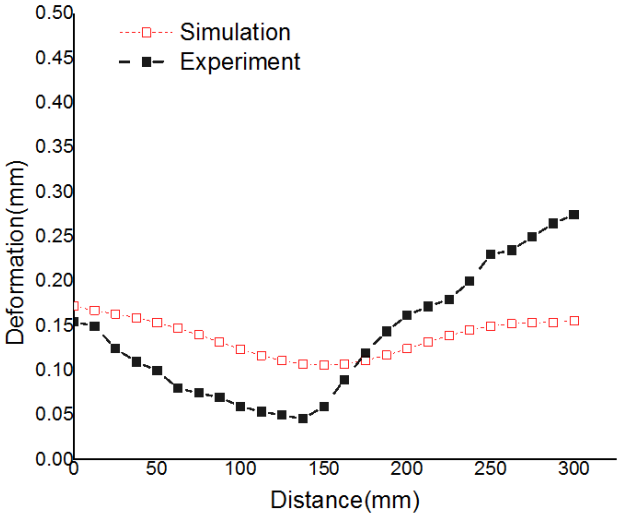

Figure 10. Simulated plate deformation in process 2A.

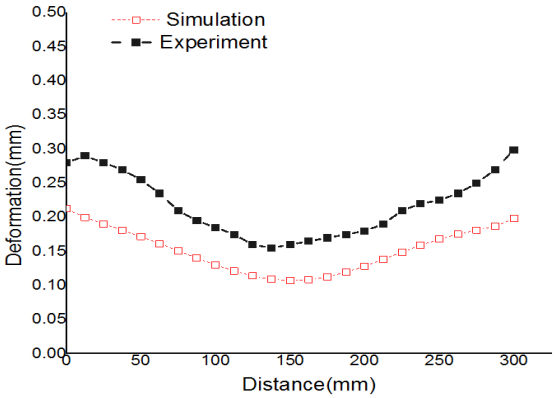

Figure 11. Simulated plate deformation in process 2B.

The simulation accuracy was verified in the experimental runs of the four GMAW processes. After performing each process 10 times, the average deformation on the box surface was measured and compared with the simulation result. The experimental and simulation results are compared in Figures 8–11.

The simulations and experiments were qualitatively consistent, but quantitatively differed by approximately 0.1 mm. This difference is attributable to the heat transfer coefficient and heat conductivity of the plate's material. These parameters were idealized in the simulation, but they will certainly be non-ideal in the experiment. In particular, the heat transfer is slowed in the real material; hence, at the end of the welding cycle, the temperature is higher on the real plate than on the simulated plate. Consequently, the deformations are lower in the simulation than in the experiment.

IV. Conclusions

This study investigated GMAW of four metal plates, forming a rectangular box structure. The box deformations were observed and compared under four GMAW processes. The following conclusions were drawn from the study:

- For the same welding parameters, the four processes yielded similar deformation profiles.
- The two double-welding processes yielded the same deformation profiles, and double welding was superior to single welding.
- The simulated temperature and stress distributions explained the deformation differences among the four processes.
- The accuracy of the simulated deformation was verified in comparisons with the experimental results.

References

[1] T. L. Teng, and P.H. Chang, A study of residual stresses in multi-pass girth-butt welded pipes, *International Journal of Pressure Vessels and Piping, 74 (1),* 1997, 59–70.

[2] P. Duranton, J. Devaus, and V. Robin, 3D modelling of multipass welding of a 316L stainless steel pipe, *Journal of Materials Processing Technology, 153 – 154,* 2004, 457– 463.

[3] B. Brickstad, and B.L. Josefson, A parametric study of residual stresses in multi-pass butt-welded stainless steel pipes, *International Journal of Pressure Vessels and Piping, 75 (1),* 1998, 11 – 25.

[4] P.J. Bouchard, and D. George, Measurement of the residual stresses in a stainless steel pipe girth weld containing long and short repairs, *International Journal of Pressure Vessels and Piping, 105 (4),* 2005, 81–91.

[5] C.D. Elcoate, R.J. Dennis, and P.J. Bouchard, Three dimensional multi-pass repair weld simulation, *International Journal of Pressure Vessels and Piping, 82 (4),* 2005, 244 – 257.

[6] J.R. Cho, B.Y. Lee, and Y.H. Moon, Investigation of residual stress and post weld heat treatment of multi-pass welds by finite element method and experiments, *Journal of Materials Processing Technology, 155 – 156,* 2004, 1690–1695.

[7] S. Murugan, K. Sanjai, B. Rai, and P.V. Kumar, Temperature distribution and residual stresses due to multipass welding in type 304 stainless steel and low carbon steel weld pads, *International Journal of Pressure Vessels and Piping, 78 (4),* 2001, 307–317.

[8] H. Bergmann, and R. Hilbinger, Numerical simulation of centre line hot cracks in laser beam welding of aluminum close to the sheet edge, *International seminar 4th, Numerical analysis of weld ability, Institute of material*, 1998, 658-668.

[9] Z.L. Feng, T. Zagharia, and S.A. David, Thermal stress development in a nickel based super alloy during weld ability test, *Welding Journal, 76,* 1997, 470–483.

[10] J.A. Goldak, and M. Akhlaghi, Computational welding Mechanics, *Springer Publishers, New York, USA*, 2005.

[11] Z.B. Dong, and Y.H. Wei, Three dimensional modeling weld solidification cracks in multipass welding, *Theoretical and Applied Fracture Mechanics, 46 (2),* 2006, 56–165.

Pham Son Minh Welding Deformation of a Rectangular Box during Gas Metal Arc Welding." IOSR Journal of Mechanical and Civil Engineering (IOSR-JMCE) , vol. 14, no. 6, 2017, pp. 85-91.